Petroleum Science 23 (2026) 4336–4348

Contents lists available at ScienceDirect

Petroleum Science

journal homepage: www.keaipublishing.com/en/journals/petroleum-science

Original Paper

CO_2-promoted Cr redox cycle driven ethane catalytic oxidative dehydrogenation to ethylene and its comparative study to ethane direct catalytic dehydrogenation

Mu-Fan Niu, Qi-Yu Sun, Yu-Hang Tan, Hai-Tao An, Han Yang, Ying Cui, Chun-Ming Xu, Bao-Jian Shen *

State Key Laboratory of Heavy Oil Processing, College of Chemical Engineering and Environment, China University of Petroleum (Beijing), Beijing, 102249, PR China

a r t i c l e i n f o

Article history:
Received 23 May 2025
Received in revised form
16 November 2025
Accepted 27 January 2026
Available online 31 January 2026

Edited by Min Li

Keywords:
Ethane catalytic oxidative dehydrogenation
High valence chromium
Redox cycle
Carbon dioxide

a b s t r a c t

In the field of ethane conversion, Cr/ZSM-5 catalysts have received considerable attention for application in direct dehydrogenation (DH) and CO_2-assisted oxidative dehydrogenation (CO_2-ODH) reactions, which can be attributed to their excellent catalytic performance. Nevertheless, the speciation of Cr on the catalyst surface within these two reaction systems, as well as the mechanisms accounting for the observed differences in catalytic performance between them, have been scarcely reported. Here, we present a comparative study on the catalytic performance and reaction mechanism of chromium oxide-loaded high-silica ZSM-5 catalysts in two ethane transformation systems: DH and CO_2-ODH. DFT calculations reveal that the adsorption energy of ethane in the CO_2-ODH system is lower than that in the DH system, indicating that the introduction of CO_2 can facilitate ethane adsorption on the catalyst surface. Experimental and computational results demonstrate that the catalysts exhibit high activity and stability in the CO_2-ODH process, achieving an ethane conversion of 51.35 mol% and an ethylene yield of 44.05 mol%. No catalyst deactivation was observed over a 48-h reaction period. Catalysts were characterized before and after the reaction using XRD, N_2 adsorption-desorption, SEM, H_2-TPR, XPS, laser Raman, and UV-Vis. It is revealed that the superior catalytic performance of the catalysts in CO_2-ODH compared to DH is primarily attributed to the introduction of CO_2. Specifically, CO_2 promotes the redox cycle of Cr species during the catalytic reaction, maintains a higher proportion of Cr^{6+} in the catalysts, and enhances the dispersion of Cr on the support surface. This work is expected to provide new insights into the effects of CO_2 on Cr species in CO_2-ODH reaction system.
© 2026 The Authors. Publishing services by Elsevier B.V. on behalf of KeAi Communications Co. Ltd. This is an open access article under the CC BY-NC-ND license (http://creativecommons.org/licenses/by-nc-nd/4.0/).

1. Introduction

As one of the most highly demanded basic chemicals globally, ethylene plays a pivotal role in the petrochemical industry, serving as a key feedstock for numerous downstream products. Currently, ethylene production processes are well-established and diverse, with three primary technological routes: ethylene production via naphtha steam cracking, coal-based ethylene synthesis, and ethylene production from light alkanes. The rapid development of the shale gas industry has significantly enhanced the cost-effectiveness and accessibility of ethane. Consequently, ethane dehydrogenation to produce ethylene has emerged as the most promising process route for ethylene production in the current context (Najari et al., 2021). However, the direct dehydrogenation of ethane to ethylene faces challenges including high reaction temperatures, insufficient ethylene selectivity, coke deposition, metal sintering, and excessive metal reduction. To overcome these technical challenges, numerous studies have proposed the selective oxidative dehydrogenation of ethane to ethylene as a promising alternative process, where diverse oxidants (i.e., O_2, CO_2, N_2O) are utilized to improve reaction performance (Alamdari et al., 2021; Dai et al., 2021).

Among the diverse oxidants investigated for the oxidative dehydrogenation of ethane to ethylene, carbon dioxide (CO_2) has

* Corresponding author.
E-mail address: baojian@cup.edu.cn (B.-J. Shen).
Peer review under the responsibility of China University of Petroleum (Beijing).

https://doi.org/10.1016/j.petsci.2026.01.045
1995-8226/© 2026 The Authors. Publishing services by Elsevier B.V. on behalf of KeAi Communications Co. Ltd. This is an open access article under the CC BY-NC-ND license (http://creativecommons.org/licenses/by-nc-nd/4.0/).

garnered substantial attention in recent studies, attributed to its characteristic as a mild oxidant. CO_2 influences the reaction behavior of ethane dehydrogenation through distinct mechanisms. The widely accepted perspective holds that, on one hand, CO_2 accelerates the reverse water-gas shift reaction (RWGS: $CO_2 + H_2 \rightarrow CO + H_2O$)— a process that reduces the partial pressure of H_2, shifting the ethane dehydrogenation equilibrium to the right. On the other hand, CO_2 mitigates coke formation via the Boudouard reaction ($CO_2 + C \rightarrow 2CO$), effectively eliminating carbon deposits that deactivate catalysts (Cheng et al., 2015; Zheng et al., 2024; Guo et al., 2022). In practice, the content of CO_2 in the reaction system also serves as a rather critical factor affecting the performance of the ethane dehydrogenation reaction. An excessive amount of CO_2 in the reaction system can trigger two unfavorable side reactions: the dry reforming reaction of ethane (DRM: $C_2H_6 + 2CO_2 \rightarrow 4CO + 3H_2$) and the non-selective cracking of ethane ($C_2H_6 \rightarrow 2C + 3H_2$). These side reactions subsequently generate undesirable by-products, such as carbon monoxide (CO) and surface coke deposits (Li et al., 2021; Tian et al., 2022). Studies have shown that the CO_2 concentration in the feedstock directly modulates the valence state of cobalt species in the catalyst: at elevated CO_2 levels, cobalt nanoparticles are prone to reduction into Co^0, a species with strong reactivity for C–C bond cleavage (promoting side reactions). Conversely, when CO_2 content is low, the catalyst predominantly retains Co^{2+} ions, which is conducive to enhancing both reaction stability and ethylene selectivity (Zheng et al., 2024). Furthermore, research suggests that CO_2 could improve the stability of reactions by stabilizing metal species or providing reactive oxygen species (Zheng et al., 2023a, 2023b). In summary, CO_2 acts as a double-edged sword in the ethane dehydrogenation process. Effectively enhancing its beneficial effects on this reaction has become one of the key research priorities in the field.

In supported CrO_x-based catalysts, chromium species exhibit multiple valence states, including Cr^{6+}, Cr^{5+}, Cr^{3+}, Cr^{2+}, and crystalline Cr_2O_3. This diversity in chromium valence states has sparked debates regarding the catalytic active sites. A majority of studies suggest that, in the catalytic dehydrogenation of light alkanes, the active species are Cr^{3+} and Cr^{6+}. In contrast, crystalline Cr_2O_3—an inherent component of the catalysts—exhibits no catalytic activity toward the target dehydrogenation reaction (Igonina et al., 2023; Baek et al., 2012). The deactivation of CrO_x-based catalysts is generally attributed to three primary factors: coke deposition on active sites, irreversible loss of active metal species, and agglomeration of chromium species (Rahmani et al., 2017; Wang et al., 2022a,b). Additionally, studies have demonstrated that chromium carbide is generated during the reaction process involving chromium species, which leads to the deactivation of the catalysts (Mashkin et al., 2023). CO_2 can modulate the chemical state of chromium species on Cr-based catalysts, thereby enhancing the reactivity and stability of the ethane dehydrogenation reaction. A key underlying mechanism is its promotion of the interconversion between Cr^{6+} and highly dispersed Cr^{3+} on the catalysts, as described by the reaction: $Cr^{3+}O_{x-1} + CO_2 \rightarrow Cr^{6+}O_x + CO$ (Numan et al., 2020). During this process, the dispersion of CrO_x on the catalysts surface was also enhanced, which is equally crucial for maintaining high reaction activity. Further research using DFT calculations and EXAFS spectroscopy has revealed that the promotion effect of CO_2 in ethane dehydrogenation stems from subtle changes in Cr–O bond length within the local coordination environment of the active sites (Zhou et al., 2024). To summarize, a large body of research has demonstrated that CO_2 exerts a significant promotional effect on the dehydrogenation of light alkanes over CrO_x-based catalysts. In contrast, two critical aspects remain inadequately addressed: the mechanism that regulates the dehydrogenation reaction under CO_2 atmosphere, and the influence of CO_2 on the active chromium species throughout the reaction process.

In this work, a systematic comparative study was performed on the catalytic performance of high-silica ZSM-5-supported catalysts with varying chromium oxide loadings. The catalysts were evaluated in two reactions: the direct dehydrogenation of ethane and the CO_2-assisted oxidative dehydrogenation of ethane. Additionally, the reaction mechanism of ethane dehydrogenation was investigated under both CO_2-free and CO_2-containing conditions. The adsorption energies of ethane in the DH and CO_2-ODH reaction systems were calculated separately using DFT. XRD, N_2 adsorption, H_2-TPR, XPS, laser Raman and UV-Vis were used to characterize the catalysts. By analyzing the coordination environment and existing state of Cr species on the catalysts, this study specifically investigated the effect of CO_2 introduction on the active Cr species. Additionally, the influence of the silica-to-alumina ratio of the ZSM-5 support on the reaction performance was examined.

2. Experimental section

2.1. Catalyst preparation

Loaded chromium oxide catalysts were prepared by impregnation method using $Cr(NO_3)_3 \cdot 9H_2O$ (99%, Aladdin) as precursor and high-silica ZSM-5(475) as support. The impregnated samples were dried overnight at 110 °C and then calcined in air at a heating rate of 4 °C/min to 550 °C for 4 h. The resulting catalysts are designated *x*Cr/ZSM-5(475) catalysts, where *x* represents the weight percentage of Cr_2O_3 in the catalysts, 4Cr/ZSM-5(35) catalyst was prepared on a ZSM-5(silica-to-alumina ratio is 35) support by the same method described above.

2.2. Characterization

The structure and surface properties of the catalysts were investigated through a series of characterization techniques. The conversion of C_2H_6 and CO_2, the selectivity and yield of C_2H_4 were calculated. The detailed characterization and catalytic evaluation are described in the Supporting Information.

2.3. Activity evaluation

The performance evaluation of catalysts for the catalytic dehydrogenation of ethane to ethylene was conducted in a small-scale fixed-bed reactor, and the experimental setup is shown in Fig. S1. The conversion of C_2H_6 and CO_2, the selectivity and yield of C_2H_4 were calculated. The detailed catalytic evaluation was described in the Supporting Information.

2.4. Computational methodology

The Vienna-Abinitio Simulation Package (VASP) was used to perform the quantitative calculations. The detailed calculation method was described in the Supporting Information.

3. Results and discussion

3.1. Catalyst characterization

3.1.1. XRD and textural property characterization

The crystal structure of the *x*Cr/ZSM-5 catalysts was determined by XRD patterns, as presented in Fig. 1(a). Typical diffraction peaks corresponding to the MFI structure are observed at

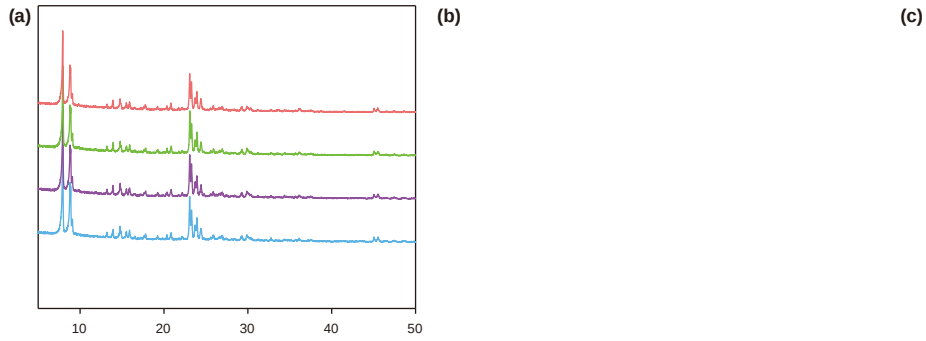

Fig. 1. **(a)** XRD, **(b)** N_2 adsorption-desorption isotherm, and **(c)** pore size distribution of *x*Cr/ZSM-5(475) catalysts.

$2\theta = 8.0°$, 8.9°, 23.1°, 23.4° and 24.0° (Guo et al., 2022). However, the intensity of these characteristic peaks decreases slightly with increasing Cr loading. No characteristic diffraction peaks of chromium oxide are detected in the XRD patterns. Two plausible explanations account for this phenomenon: first, chromium species are highly dispersed on the ZSM-5 support; second, chromium oxide exists as ultra-fine particles, that are too small to be detected by XRD. To determine the elemental composition of the *x*Cr/ZSM-5 catalysts, X-ray fluorescence spectroscopy (XRF) was employed for elemental analysis. The results obtained from this analysis are provided in Table S1. Elemental analysis data indicate that the actual loading of chromium oxide in each target catalyst is in good agreement with the corresponding theoretical values.

Nitrogen adsorption-desorption isotherms and pore size distributions for the catalysts with varying Cr loadings are shown in Fig. 1(b) and (c), respectively. Notably, all these catalysts exhibit Type IV adsorption-desorption isotherms, a feature typical of microporous materials. Owing to the capillary condensation of N_2, the relative pressure (P/P_0) increases sharply within the narrow range of 0.1–0.25. This sharp increase indicates the presence of uniformly distributed small microporous in the catalysts. As reported in previous studies, ordered microporous channels with uniform pore structures can form favorable interactions with chromate ions. This interaction is beneficial for stabilizing and dispersing the active chromium species (Yang et al., 2022). The textural properties of the catalysts are presented in Table 1. Analysis of these data reveals a clear trend: the specific surface area of the catalysts decreases progressively as the chromium loading increases. Notably, the 6Cr/ZSM-5(475) catalyst exhibits a more pronounced reduction in specific surface area. This observation further suggests that metal species are prone to agglomeration in catalysts with high metal loading. Two adverse effects arise from this agglomeration: first, it obstructs part of the pore channels, limiting reactant diffusion; second, it lowers the dispersion of active metal species, which in turn leads to reduced catalytic activity.

Table 1
Textural property of catalysts with different Cr contents.

Sample	S_{BET}, m^2/g	S_{micro}, m^2/g	S_{ext}, m^2/g	V_{total}, cm^3/g	V_{micro}, cm^3/g	V_{meso}, cm^3/g
ZSM-5(475)	386	152	234	0.223	0.078	0.146
1Cr/ZSM-5(475)	383	149	234	0.220	0.075	0.145
2Cr/ZSM-5(475)	377	152	225	0.218	0.075	0.143
4Cr/ZSM-5(475)	374	145	233	0.218	0.072	0.146
6Cr/ZSM-5(475)	361	136	226	0.210	0.068	0.143
4Cr/ZSM-5(475)-ODH	358	184	174	0.213	0.088	0.125
4Cr/ZSM-5(475)-DH	335	195	140	0.201	0.095	0.106

3.1.2. OH-IR and Cr OH interaction characterization

To explore the interaction mechanism between Cr species and the high-silica ZSM-5 support, a comparative analysis of the IR spectra of catalysts with varying Cr loadings was conducted, focusing on the hydroxyl stretching vibration region (3800–3200 cm^{-1}). Prior to spectral acquisition, all samples were subjected to a pretreatment step: heating at 400 °C for 2 h under flowing nitrogen. This pretreatment was intended to eliminate the influence of moisture, ensuring the accuracy of the subsequent spectral measurements. As shown in Fig. 2(a), distinct characteristic signals are observed for all samples, which can be assigned to two types of Si hydroxyl groups: isolated terminal Si hydroxyl groups (at 3720 cm^{-1}) and Si hydroxyl groups at structural defects (at 3500 cm^{-1}) (Guo et al., 2022; Cheng et al., 2017). These characteristic hydroxyl peaks are attributed to the formation of complexes between chromium species and surface Si hydroxyl groups on the ZSM-5 support. This result clearly demonstrates that Cr species preferentially anchor to the vicinity of isolated terminal Si hydroxyl groups and Si hydroxyl groups associated with structural defects. The strong anchoring of Cr species to the –OH groups on the catalyst support surface plays a key role in facilitating the improved dispersion of CrO_x species. As evident from Fig. 2(a), a gradual reduction in the intensity of these characteristic hydroxyl peaks is observed as the chromium loading of the catalysts increases. At excessively high chromium loadings, a fraction of the chromium species fails to form interactions with surface hydroxyl groups. Instead, these chromium species tend to aggregate into chromium oxide agglomerates, and this agglomeration further impedes the coordination reaction between chromium and hydroxyl groups.

3.1.3. H_2-TPR, XPS and redox capacity of the Cr species

The H_2-TPR profiles (Fig. 2(b)) reflect the redox properties of chromium species on the catalysts. As observed in the H_2-TPR profiles, all catalysts display a pronounced reduction peak around 420 °C, accompanied by a shoulder peak at 297 °C. These two peaks are collectively attributed to the reduction of Cr^{6+} to Cr^{3+} (Cai et al., 2024). As chromium loading increases, the reduction peak near 420 °C exhibits a downward temperature shift, which is indicative of a certain degree of agglomeration among the chromium species on the catalysts. It is evident that as chromium loading increases, a portion of the chromium species fails to coordinate with the Si hydroxyl groups on the ZSM-5 support, indicating weakened interaction between the metal species and the

Cr species partially cover the acid sites on the ZSM-5(475) support (Wang et al., 2024).

3.2. Evaluation of catalytic performance

3.2.1. Direct dehydrogenation of ethane (DH)

The performance evaluation results of the DH reaction over catalysts with different chromium loadings are presented in Fig. 3(a). It can be observed that ethane conversion over the Cr/ZSM-5(475) catalysts increase significantly with increasing chromium loading at low loadings. However, the conversion ceases to increase when the loading rises from 4 to 6 wt%. All Cr/ZSM-5(475) catalysts exhibit high ethylene selectivity, a phenomenon that is also reflected in the carbon balance data shown in Fig. S2. As indicated by the deactivation rate data in Fig. 3(b) (Deactivation rate constant $= \frac{\text{Conversion at 12 min} - \text{Conversion at 305 min}}{\text{Conversion at 12 min}} \times 100\%$), all catalysts undergo rapid deactivation. Importantly, this deactivation behavior becomes more pronounced at higher chromium loadings, with a marked increase in the deactivation rate constant observed under these conditions. The possible causes of catalyst deactivation include carbon deposition, metal sintering, and irreversible metal reduction (Wang et al., 2023; Yadav et al., 2024).

3.2.2. CO_2-assisted oxidative dehydrogenation of ethane (CO_2-ODH)

Subsequently, the reaction behavior of CO_2-assisted oxidative dehydrogenation of ethane (CO_2-ODH) over the catalysts was investigated, using a feed gas mixture consisting of 5 mol% ethane, 5 mol% CO_2, and 90 mol% N_2. The performance of the blank ZSM-5(475) support in the ODH and DH reactions was first examined, with the results presented in Fig. S3. The conversion of both ethane and CO_2 over this support $\leq$1 mol%. This result reveals two key points: first, the ZSM-5(475) support itself cannot promote the conversion of ethane or CO_2, confirming that the catalytic activity of the system stems from the loaded Cr species; second, thermodynamic factors can be excluded from the ethane conversion process. The catalytic performance of the 4Cr/ZSM-5(475) catalyst for DH and CO_2-ODH is shown in Fig. 3(c) and (d). Over a 22-h reaction duration, the catalyst underwent significant deactivation in the DH reaction, as reflected by the decrease in ethane conversion from an initial 37.57 mol% to a final 20.95 mol%. In the ODH reaction, the addition of CO_2 reduces ethylene selectivity. This is because CO_2 can react with ethane through two distinct pathways: (1) $C_2H_6 + CO_2 \rightarrow C_2H_4 + CO + H_2O$; (2) $C_2H_6 + 2CO_2 \rightarrow 4CO + 3H_2$ (Chen et al., 2020; Zhang et al., 2024). As revealed by thermodynamic calculations, both of the aforementioned reactions are thermodynamically feasible at temperatures exceeding 550 °C, with ethylene and synthesis gas as the main products (Bugrova et al., 2019). The introduction of 5 mol% CO_2 into the reaction system led to a significant enhancement in ethane conversion. Notably, over the entire 48-h investigation period, no deactivation of the catalyst was detected, with detailed experimental data presented in Table S2 of the Supporting Information.

It is generally accepted by researchers that crystalline Cr_2O_3 inherently present in CrO_x-based catalysts is inert toward the dehydrogenation of light alkanes. Conversely, Cr^{6+} species in the catalyst and coordinately unsaturated Cr^{3+}—generated through the reduction of Cr^{6+}—are typically identified as the effective active sites for this reaction (Al-Awadi et al., 2021). Thus, the initial content and dispersion of Cr^{6+} species in CrO_x-based catalysts are key factors that significantly affect the catalytic performance of the dehydrogenation reaction. The catalytic performance of catalysts with different chromium loadings in ODH and DH reactions, together with the quantitative correlation between the performance and the Cr^{6+}/Cr^{3+} atomic ratio of the catalysts, is illustrated in Fig. 3(e). Within the Cr/ZSM-5(475) catalyst system, the Cr^{6+}/Cr^{3+} atomic ratio initially increases and subsequently decreases with the gradual increase in chromium loading, with the highest value observed in the 4Cr/ZSM-5(475) catalyst. Notably, in both

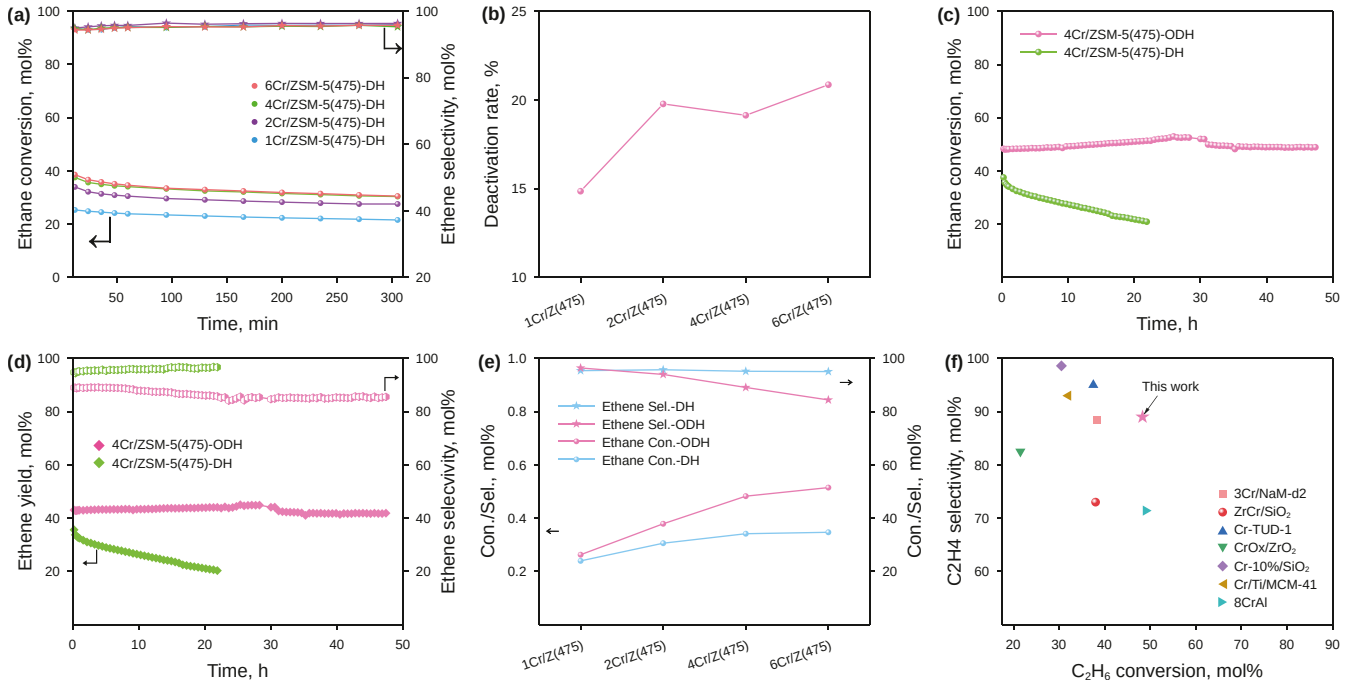

Fig. 3. **(a)** Ethane conversion and Ethylene selectivity in the DH reaction, **(b)** deactivation rate constant in the DH reaction, **(c)** ethane conversion on 4Cr/ZSM-5(475) catalyst in DH and ODH reactions, **(d)** ethylene yield and selectivity on 4Cr/ZSM-5(475) catalyst in DH and ODH reactions, **(e)** quantitative correlation between reaction performance and Cr^{6+}/Cr^{3+} atomic ratio in the catalysts, **(f)** ethane dehydrogenation performance on different CrO_x-based catalysts (see Table S3) of *x*Cr/ZSM-5(475) catalysts.

ethane DH and ODH reactions, the trend of ethane conversion with chromium loading shows two distinct stages: below 4 wt% loading, conversion increases rapidly; above 4 wt% loading, the increase in conversion is merely marginal. As illustrated in Fig. 4(a), the observed slight increase in overall conversion is attributed to the dry reforming reaction. In contrast, the conversion of the target dehydrogenation reaction even experiences a marginal decrease. Ethylene selectivity shows a more pronounced difference between the DH and ODH reactions. In the DH reaction, ethylene selectivity remains consistently high and varies slightly with changes in metal loading. In the ODH reaction, ethylene selectivity exhibits an overall decreasing trend with increasing chromium loading. Notably, the ethylene selectivity declines markedly when the loading exceeds 4 wt%. For the dehydrogenation of ethane over Cr/ZSM-5(475) catalysts, the initial content of Cr^{6+} species exhibits a positive correlation with the catalytic activity of the reaction, but this relationship is limited to Cr loadings below 4 wt%. A further increase in chromium loading does not necessarily result in improved catalytic performance. When the chromium loading surpasses 4 wt%, the initial content of Cr^{6+} species starts to decline, which is accompanied by a notable decrease in ethylene selectivity. This behavior is likely attributable to the poor dispersion of CrO_x species in the catalysts, with a portion of chromium species aggregating into agglomerates or further converting into inactive crystalline Cr_2O_3. To explicitly demonstrate the superior performance of the 4Cr/ZSM-5(475) catalyst, the performance of different CrO_x-based catalysts in ethane dehydrogenation is compiled in Fig. 3(f) and Table S3. Notably, the 4Cr/ZSM-5(475) catalyst achieves an initial ethane conversion of 49 mol% while retaining a high ethylene selectivity of 89.1 mol%.

Fig. 4(a) demonstrates that, in the ODH reaction, CO_2 conversion increases significantly with increasing Cr loading, accompanied by overall upward trend in the proportion of the dry reforming reaction. This trend is especially prominent when the Cr loading is increased from 4 to 6 wt%, at which point the catalytic activity of the dry reforming reaction is significantly enhanced. By integrating the results of H_2-TPR and XPS characterization, it is inferred that the relatively poor dispersion of CrO_x within the catalysts is conducive to promoting the dry reforming reaction. It can be observed that the CO_2 conversion of the Cr/ZSM-5(475) catalysts in the ODH reaction is significantly lower than that of ethane. This indicates a relatively small proportion of the dry reforming reaction, with ethane conversion occurring primarily via direct dehydrogenation. Through thermodynamic calculations, Bugrova et al. (2019) found that the ΔG of ethane direct dehydrogenation ($C_2H_6 \rightarrow C_2H_4 + H_2$) is comparable to that of CO_2-assisted ethane dehydrogenation ($C_2H_6 + CO_2 \rightarrow C_2H_4 + CO + H_2O$). Analyzing the product composition facilitates a more in-depth understanding of the reaction pathway for ODH. Fig. 4(b) and (c) present the H_2/C_2H_4 and CO/C_2H_4 molar ratios in the products of ODH and DH reactions, obtained from catalysts with different chromium loadings. The theoretical H_2/C_2H_4 molar ratio for ethane direct dehydrogenation products should be 1. However, this ratio exceeds 1 in practical reactions, primarily due to side reactions—such as ethane C–C bond cleavage, which forms carbon deposits and hydrogen. Fig. 4(b) reveals that for all catalysts, the H_2/C_2H_4 molar ratio in the ODH reaction is both lower than that in the DH reaction and close to 1. This key observation confirms that the RWGS reaction — ($CO_2 + H_2 \rightarrow H_2O + CO$) — takes place in the ODH reaction, and this reaction shifts the overall reaction equilibrium toward ethylene formation (Meng et al., 2024; Tedeeva et al., 2022). For the CO_2-assisted oxidative dehydrogenation of ethane, the expected CO/C_2H_4 molar ratio in the products is theoretically 1. However, experimental data from Fig. 4(c) indicate that this ratio is notably less than 1. To summarize, the Cr/ZSM-5(475) catalysts do not exhibit ideal behavior for either direct dehydrogenation or oxidative dehydrogenation in the ODH reaction. Nevertheless, the H_2/C_2H_4 molar ratio in the ODH reaction is very close to 1, leading to the conclusion that ethane direct dehydrogenation predominates, while the RWGS reaction makes a notable contribution.

The effect of temperature on the performance of the ODH and DH reactions over the 4Cr/ZSM-5(475) catalyst is shown in Fig. 5(a)–(c). When the reaction temperature is lower than 620 °C, the rate of increase in ethane conversion is relatively sluggish as the temperature gradually rises. When the reaction temperature is elevated from 620 to 650 °C, the rate of increase in ethane conversion becomes notably more pronounced. Ethylene selectivity decreases slightly with increasing temperature, while ethylene yield shows a positive correlation with reaction temperature. Within the temperature range of 580–650 °C, the apparent activation energies for ethane conversion in ODH and DH reactions over the 4Cr/ZSM-5(475) catalyst were calculated via the Arrhenius equation, and the results are presented in Fig. 5(b). The apparent activation energy for ethane conversion in the ODH reaction is 97 kJ/mol, which is lower than the value of 113 kJ/mol for the DH reaction. This indicates that ethane conversion occurs more readily in the ODH reaction.

Fig. 5(d) shows the influence of ethane space velocity on the ODH catalytic performance of the 4Cr/ZSM-5(475) catalyst. The residence time of the feed gas on the catalyst surface was adjusted by changing the catalyst weight. With an increase in ethane space velocity, the residence time of ethane molecules on the catalyst surface decreases, causing a reduction in ethane conversion. Nevertheless, this reduced residence time simultaneously

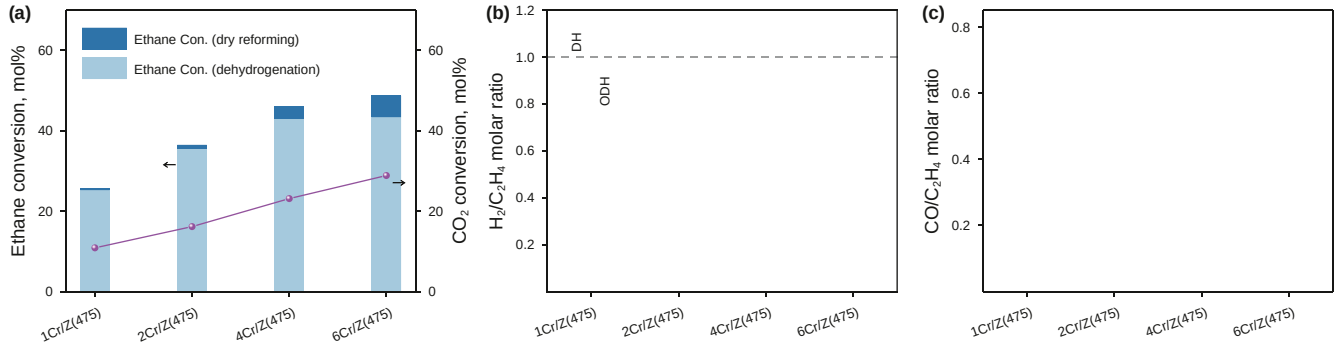

Fig. 4. **(a)** Ethane and CO_2 conversion in the ODH reaction, **(b)** H_2/C_2H_4 molar ratio, **(c)** CO/C_2H_4 molar ratio of *x*Cr/ZSM-5(475) catalysts in DH and ODH reactions. Reaction conditions: 650 °C, 0.1 MPa, 6000 mL/(g□h), 5 mol% C_2H_6.

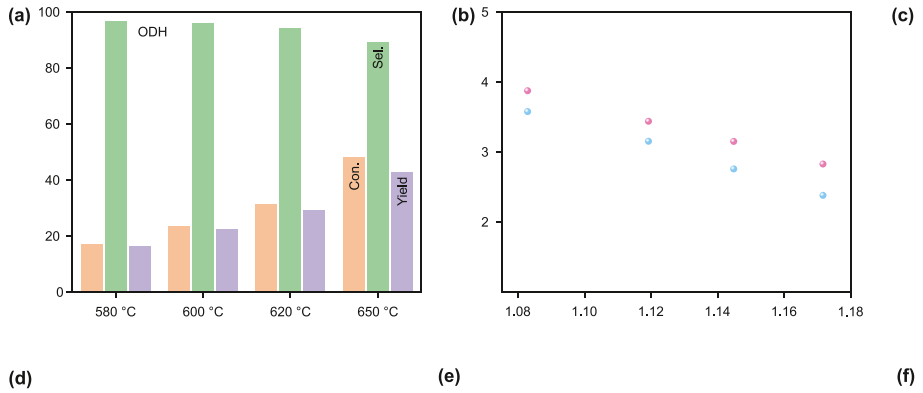

Fig. 5. **(a)** Effect of temperature on the ODH reaction, **(b)** activation energies for ethane conversion in ODH and DH reactions, **(c)** effect of temperature on the DH reaction, **(d)** effect of space velocity on the ODH reaction, the horizontal axis represents the space velocity of the feed gas (mL/(g□h)), **(e)** effect of CO_2/C_2H_6 molar ratio in the feed, the horizontal axis represents the CO_2/C_2H_6 molar ratio in the feed gas, **(f)** effect of ethane content in the feed, the horizontal axis represents the molar ratio of C_2H_6 in the feed gas of 4Cr/ZSM-5(475) catalyst.

suppresses the deep cracking of ethane, thereby increasing ethylene selectivity. Fig. 5(e) presents the influence of the CO_2/C_2H_6 molar ratio on the ODH reaction performance. When the CO_2/C_2H_6 molar ratio is increased from 0 to 4, there is a notable increase in ethane conversion (from 35.67 to 53.10 mol%)—accompanied by a decrease in ethylene selectivity (from 94.44 to 80.76 mol%). This confirms that the introduction of CO_2 exerts a marked enhancing effect on ethane conversion. However, the dry reforming reaction that involve ethane occur during the process, leading to a certain degree of reduction in ethylene selectivity. The effect of ethane content on reaction performance in the ODH reaction—with the CO_2/C_2H_6 molar ratio kept constant at 1—is presented in Fig. 5(f). When ethane content is increased from 5 to 30 mol%, there is a decrease in both ethane conversion (from 48.07 to 28.73 mol%) and ethylene selectivity (from 89.00 to 82.39 mol%). It is well established that increasing ethane content shifts the reaction equilibrium away from ethane conversion. Consequently, both ethane conversion and ethylene selectivity decrease as ethane content rises (Li et al., 2025; Jiang et al., 2024).

3.3. Mechanism of CO_2 enhancing reaction stability

Fig. 6(a) shows the XRD patterns of the 4Cr/ZSM-5(475) catalyst following the DH and ODH reactions, respectively. Specifically, after the DH reaction, the intensity of the catalyst's characteristic XRD peaks decreased slightly, though their positions remained unaltered. Fig. 6(b) and (c) show the nitrogen adsorption-desorption isotherms and pore size distribution of the 4Cr/ZSM-5(475) catalyst post-reaction, respectively, while the corresponding data are summarized in Table 1. Notably, the specific surface area and mesoporous volume of the catalyst decreased post-reaction, and this reduction was more pronounced in the DH reaction compared to the ODH reaction. This decrease can be attributed to two possible factors: carbon deposit formation during the reaction, or pore obstruction by crystalline Cr_2O_3 generated on the catalyst surface. The TG curve in Fig. 6(d) shows that the carbon deposits after the ODH reaction are lower than that after the DH reaction. This difference may be attributed to the Boudouard reaction ($CO_2 + C \rightarrow 2CO$) between CO_2 and carbonaceous species generated during the ODH reaction (Numan et al., 2021; Myint et al., 2016). Nevertheless, the carbon deposition amount in the DH reaction is not sufficient to induce catalyst deactivation. This observation implies that the primary role of CO_2 is not to initiate the Boudouard reaction. Fig. 7 presents the SEM-EDS images of the 4Cr/ZSM-5(475) catalyst after reaction. Notably, the metal exhibits uniform distribution on both the fresh catalyst and the catalyst post-reaction, and no metal cluster particles are detected. This observation confirms that no significant metal sintering took place on the catalysts (Wang et al., 2023; Tian et al., 2024).

During the reaction, ethane is initially adsorbed onto Cr species, located near Si hydroxyl groups. When CO_2 is absent, the initial stage of the dehydrogenation reaction proceeds in two steps: first, oxidative dehydrogenation catalyzed by Cr^{6+} sites, second, direct dehydrogenation catalyzed by Cr^{3+} sites. Notably, the reaction rate of the Cr^{6+}-catalyzed oxidative pathway is significantly greater than that of the Cr^{3+} catalyzed direct pathway. Research indicates that tetrahedral Cr^{6+} is reduced to octahedral Cr^{3+} during the reaction, while octahedral Cr^{3+} aggregates as the reaction progresses (Shishido et al., 2012). The aggregation of Cr^{3+} reduces catalyst activity, leading to a rapid decline in ethane conversion. For CO_2-assisted oxidative dehydrogenation of ethane, the addition of CO_2 enhances the redox cycle involving the interconversion between tetrahedral Cr^{6+} and octahedral Cr^{3+}. The mechanism of ethane direct dehydrogenation is illustrated in Fig. 8(a). In the initial stage, ethane undergoes oxidative dehydrogenation while Cr^{6+} is reduced to Cr^{3+}. Since Cr^{3+} cannot be re-oxidized to Cr^{6+}, subsequent dehydrogenation reactions only proceed on Cr^{3+} sites. The

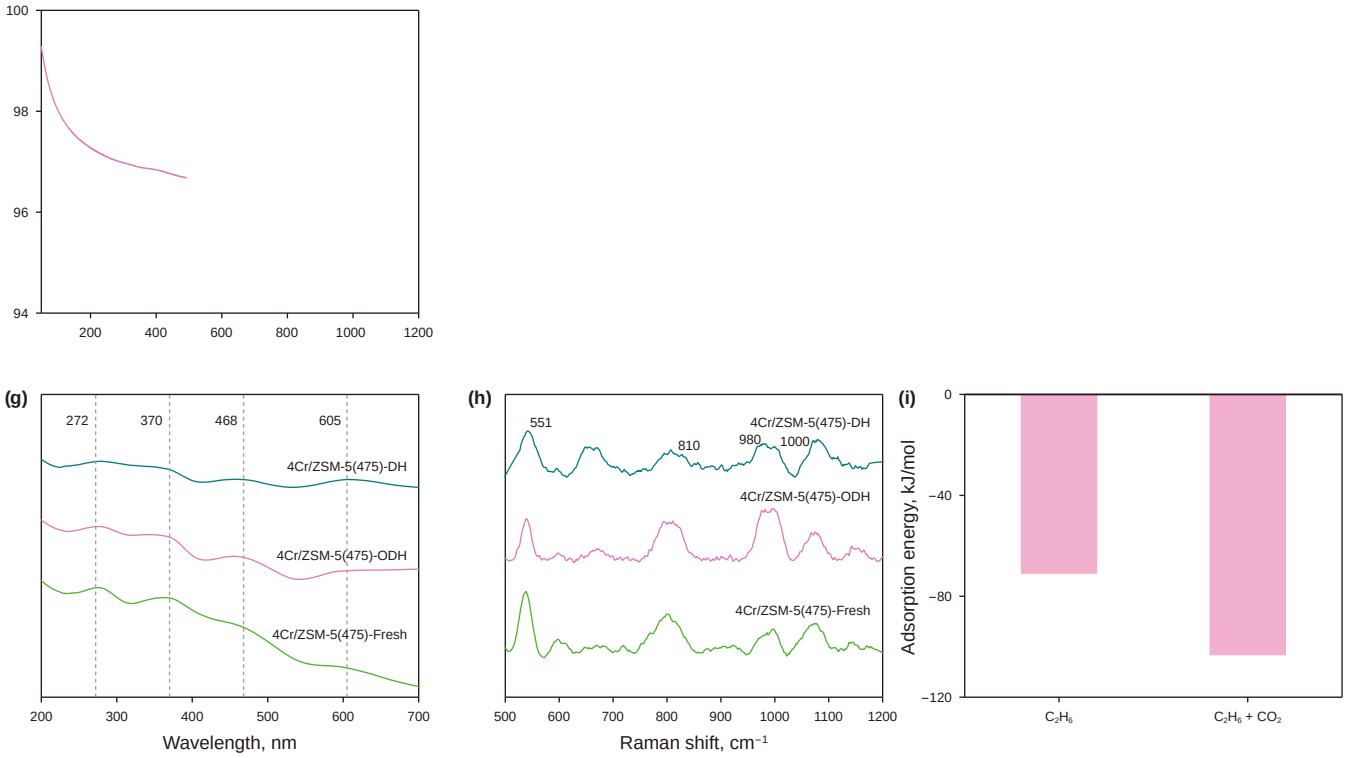

Fig. 6. Following the DH and ODH reactions on the 4Cr/ZSM-5(475) catalyst, **(a)** XRD, **(b)** N_2 adsorption-desorption isotherm, **(c)** pore size distribution, **(d)** TG curve, **(e)** H_2-TPR, **(f)** XPS, **(g)** UV-Vis, **(h)** Laser Raman, **(i)** adsorption energy of ethane on Cr/ZSM-5(475) catalysts.

gradual aggregation of Cr^{3+} causes a progressive decline in catalytic activity. Fig. 8(b) illustrates the mechanism under oxidative dehydrogenation conditions with CO_2 participation. Here, a portion of Cr^{3+} is re-oxidized to Cr^{6+}, enabling ethane to proceed via two pathways: direct dehydrogenation at Cr^{3+} sites and oxidative dehydrogenation at Cr^{6+} sites. This dual-pathway reaction not only enhances the catalyst's reactivity but also suppresses Cr^{3+} aggregation, ultimately improving the reaction's stability (Wang et al., 2003; Hoffman et al., 2023; Wan et al., 2022).

The H_2-TPR profiles of the 4Cr/ZSM-5(475) catalyst before and after reaction are shown in Fig. 6(e). The H_2 reduction peak at 416 °C—corresponding to the reduction of Cr^{6+} to Cr^{3+}—shifted to 370 °C after the reaction. This indicates the formation of more easily reducible Cr polymers during the reaction. It can also be observed that the H_2 reduction peak area at 370 °C following the ODH reaction is significantly greater than that of the DH reaction. This result demonstrates that the introduction of CO_2 promotes the redox cycle of Cr species, as described by the reaction $Cr^{3+}O_{x-1} + CO_2 \rightarrow Cr^{6+}O_x + CO$, thereby maintaining a higher proportion of Cr^{6+} in the dehydrogenation reaction system (Cheng et al., 2015; Zhou et al., 2024; Franceschini et al., 2023). Fig. 6(f) and Table 2 show the XPS data of the 4Cr/ZSM-5(475) catalyst after reaction. It is observed that the Cr^{6+}/Cr^{3+} atomic ratio of the post-reaction catalyst is lower than that of the fresh catalyst. Notably, this ratio decreased more significantly after the DH than after the ODH, confirming that the ODH process retained a relatively higher proportion of Cr^{6+}. This observation is consistent with the previously obtained H_2-TPR results.

The oxidation state and coordination environment of Cr species in the 4Cr/ZSM-5(475) catalyst exert a significant impact on its catalytic activity. UV-Vis analysis provides supplementary information regarding the chemical state of Cr species, with the acquired results depicted in Fig. 6(g). Two absorption bands at approximately 272 and 370 nm were observed in both the fresh and post-reaction 4Cr/ZSM-5(475) catalyst. These bands are typically assigned to the $O^{2-} \rightarrow Cr^{6+}$ charge transfer transition, which is characteristic of tetrahedral coordinated chromate species (Wang et al., 2022a,2022b; Mashkin et al., 2022). The peak at 468 nm is

Fig. 7. SEM-EDS of **(a)**, **(b)** 4Cr/ZSM-5(475)-fresh; **(c)**, **(d)** 4Cr/ZSM-5(475)-ODH; **(e)**, **(f)** 4CrZSM-5(475)-DH.

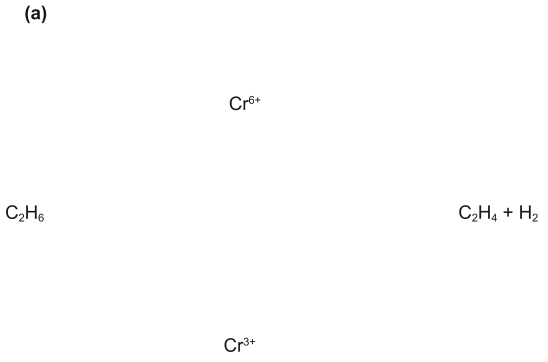

Fig. 8. Mechanism of ethane dehydrogenation reaction, **(a)** without CO_2, **(b)** with CO_2.

also attributed to Cr^{6+}, and this peak is closely associated with the distortion of tetrahedral symmetric Cr^{6+} groups. It is observed that the peak intensities at 272, 370, and 468 nm are markedly higher for the catalyst after the ODH reaction than for that after the DH reaction. This intensity difference confirms that the ODH reaction retains a larger amount of Cr^{6+} in the catalysts compared to DH reaction. Notably, the peak at 605 nm corresponds to the characteristic octahedral symmetry transition of microcrystalline chromium oxide. This peak is detected in both the catalyst after the ODH and the DH reactions, implying that the dispersion of Cr species on the post-reaction catalysts has decreased to varying extents.

Laser Raman spectra was employed to characterize the molecular properties of Cr species dispersed on the catalysts, and the corresponding results are shown in Fig. 6(h). In the Laser Raman spectroscopy of the 4Cr/ZSM-5(475) catalysts (fresh and post-reaction), a characteristic band at 551 cm^{-1} is observed. This band is assigned to Cr_2O_3 crystals, and its intensity is notably lower for the post-ODH catalyst than for the post-DH catalyst. This difference confirms that CO_2 can partially re-oxidize Cr^{3+} to Cr^{6+} during the ODH reaction, which in turn suppresses the formation of Cr_2O_3 crystals. Franceschini et al. (2023) further verified through in situ Raman analysis that, during the ethane dehydrogenation process over CrO_x/Al_2O_3 catalysts, the introduction of CO_2 enables the partial re-oxidation of Cr^{3+} to Cr^{6+}. In the spectra of all catalysts, two additional characteristic bands are observed at approximately 980 and 1000 cm^{-1}. Specifically, these bands are attributable to isolated Cr^{6+} and aggregated Cr^{6+} species, respectively. Concurrently, a band at 810 cm^{-1} appears, which is attributed to the bending mode of the Cr–O–Cr bond in polymerized chromate (Cheng et al., 2015, 2017; Karami et al., 2023). The intensity of these bands is higher in post-ODH catalyst than in post-DH catalyst. This indicates that the transformation of surface-dispersed Cr^{6+} (from monochromate and polychromate species)

Appendix A. Supplementary data

Supplementary data to this article can be found online at https://doi.org/10.1016/j.petsci.2026.01.045.

References

Al-Awadi, A.S., El-Toni, A.M., Labis, J.P., et al., 2021. Mesoporous Organo-Silica supported chromium oxide catalyst for oxidative dehydrogenation of ethane to ethylene with CO_2. Catalysts 11, 642. https://doi.org/10.3390/catal11050642.

Alamdari, A., Karimzadeh, R., Abbasizadeh, S., 2021. Present state of the art of and outlook on oxidative dehydrogenation of ethane: catalysts and mechanisms. Rev. Chem. Eng. 37, 481–532. https://doi.org/10.1515/revce-2017-0109.

Ayari, F., Mhamdi, M., Álvarez-Rodríguez, J., et al., 2013. Selective catalytic reduction of NO with NH_3 over Cr-ZSM-5 catalysts: general characterization and catalysts screening. Appl. Catal. B Environ. 134–135, 367–380. https://doi.org/10.1016/j.apcatb.2013.01.026.

Baek, J., Yun, H.J., Yun, D., et al., 2012. Preparation of highly dispersed chromium oxide catalysts supported on mesoporous silica for the oxidative dehydrogenation of propane using CO_2: insight into the nature of catalytically active chromium sites. ACS Catal. 2, 1893–1903. https://doi.org/10.1021/cs300198u.

Bugrova, T.A., Dutov, V.V., Svetlichnyi, V.A., et al., 2019. Oxidative dehydrogenation of ethane with CO_2 over CrO_x catalysts supported on Al_2O_3, ZrO_2, CeO_2 and $Ce_xZr_{1-x}O_2$. Catal. Today 333, 71–80. https://doi.org/10.1016/j.cattod.2018.04.047.

Cai, L., Zhao, Y., Tian, X., et al., 2024. Well-dispersed monolayer CrO_x/Silicalite-1 catalysts for efficient propane dehydrogenation. Chem. Eng. J. 494, 152925. https://doi.org/10.1016/j.cej.2024.152925.

Chen, X., Chen, Y., Song, C., et al., 2020. Recent advances in supported metal catalysts and oxide catalysts for the reverse water-gas shift reaction. Front. Chem. 8, 709. https://doi.org/10.3389/fchem.2020.00709.

Cheng, Y., Zhang, F., Zhang, Y., et al., 2015. Oxidative dehydrogenation of ethane with CO_2 over Cr supported on submicron ZSM-5 zeolite. Chin. J. Catal. 36, 1242–1248. https://doi.org/10.1016/s1872-2067(15)60893-2.

Cheng, Y., Zhou, L., Xu, J., et al., 2016. Chromium-based catalysts for ethane dehydrogenation: effect of SBA-15 support. Microporous Mesoporous Mater. 234, 370–376. https://doi.org/10.1016/j.micromeso.2016.07.031.

Cheng, Y., Miao, C., Hua, W., et al., 2017. Cr/ZSM-5 for ethane dehydrogenation: enhanced catalytic activity through surface silanol. Appl. Catal. A: Gen. 532, 111–119. https://doi.org/10.1016/j.apcata.2016.12.025.

Dai, Y., Gao, X., Wang, Q., et al., 2021. Recent progress in heterogeneous metal and metal oxide catalysts for direct dehydrogenation of ethane and propane. Chem. Soc. Rev. 50, 5590–5630. https://doi.org/10.1039/d0cs01260b.

Felvey, N.W., Meloni, M.J., Kronawitter, C.X., et al., 2020. Ethane dehydrogenation over Cr/ZSM-5: characterization of active sites through probe molecule adsorption FTIR. Catal. Sci. Technol. 10, 5069–5081. https://doi.org/10.1039/d0cy01022g.

Franceschini, G.D.N., Concepción, P., Schwaab, M., et al., 2023. Spectroscopic insights into the role of CO_2 on the nature of Cr species in a CrO_x/Al_2O_3 catalysts during ethane dehydrogenation with CO_2. Appl. Catal. A: Gen. 661, 119260. https://doi.org/10.1016/j.apcata.2023.119260.

Gong, W., Wang, T., Wang, L., et al., 2022. High-performance of CrO_x/HZSM-5 catalyst on non-oxidative dehydrogenation of C_2H_6 to C_2H_4: effect of supporting materials and associated mechanism. Fuel Process. Technol. 233, 107294. https://doi.org/10.1016/j.fuproc.2022.107294.

Guo, H., Miao, C., Hua, W., et al., 2020. Enhanced catalytic performance of Cr/MOR for ethane dehydrogenation through dealumination. Catal. Lett. 151, 1499–1507. https://doi.org/10.1007/s10562-020-03421-7.

Guo, H., He, H., Miao, C., et al., 2022. Ethane conversion in the presence of CO_2 over Co-based ZSM-5 zeolite: Co species controlling the reaction pathway. Mol. Catal. 519, 112155. https://doi.org/10.1016/j.mcat.2022.112155.

Hoffman, A.S., Greaney, M., Finzel, J., et al., 2023. Elucidation of puzzling questions regarding the CrO_x/Al_2O_3 catalyst I. X-ray absorption spectroscopy aided identification of the nature of the chromium oxide species in the CrO_x/Al_2O_3 dehydrogenation catalyst system. Appl. Catal. A: Gen. 660, 119187. https://doi.org/10.1016/j.apcata.2023.119187.

Igonina, M., Tedeeva, M., Kalmykov, K., et al., 2023. Properties of CrO_x/MCM-41 and its catalytic activity in the reaction of propane dehydrogenation in the presence of CO_2. Catalysts 13, 906. https://doi.org/10.3390/catal13050906.

Jiang, S., Chang, C.W., Swann, W.A., et al., 2024. Pt_3Mn/SiO_2 + ZSM-5 bifunctional catalyst for ethane dehydroaromatization. Catalysts 14, 365. https://doi.org/10.3390/catal14060365.

Karami, H., Soltanali, S., Najafi, A.M., et al., 2023. Amorphous silica-alumina as robust support for catalytic dehydrogenation of propane: effect of Si/Al ratio on nature and dispersion of Cr active sites. Appl. Catal. A: Gen. 658, 119167. https://doi.org/10.1016/j.apcata.2023.119167.

Li, X., Yang, Z., Zhang, L., et al., 2021. Effect of Pd doping in (Fe/Ni)/CeO_2 catalyst for the reaction path in CO_2 oxidative ethane dehydrogenation/reforming. Energy 234, 121261. https://doi.org/10.1016/j.energy.2021.121261.

Li, C., Meyer, R.J., Yacob, S., et al., 2025. Highly stable subnanometric PtIn clusters for the selective dehydrogenation of alkanes. ChemSusChem 18, e202401284. https://doi.org/10.1002/cssc.202401284.

Mashkin, M., Tedeeva, M., Fedorova, A., et al., 2022. CrO_x/SiO_2 mesoporous catalysts prepared using beta-cyclodextrin as a template and their catalytic properties in propane oxidative dehydrogenation in the presence of carbon dioxide. Microporous Mesoporous Mater. 338, 111967. https://doi.org/10.1016/j.micromeso.2022.111967.

Mashkin, M.Y., Tedeeva, M.A., Fedorova, A.A., et al., 2023. Synthesis of $Ce_xZr_{1-x}O_2$/SiO_2 supports for chromium oxide catalysts of oxidative dehydrogenation of propane with carbon dioxide. J. Chem. Technol. Biotechnol. 98, 1247–1259. https://doi.org/10.1002/jctb.7339.

Meng, X., Jin, F., Qiang Peng, A., et al., 2024. Influence of different Ga species in MWW zeolite bifunctional catalysts on the ethane dehydrogenation and dehydroaromatization in the absence and presence of CO_2. Fuel 363, 130968. https://doi.org/10.1016/j.fuel.2024.130968.

Myint, M., Yan, B., Wan, J., et al., 2016. Reforming and oxidative dehydrogenation of ethane with CO_2 as a soft oxidant over bimetallic catalysts. J. Catal. 343, 168–177. https://doi.org/10.1016/j.jcat.2016.02.004.

Najari, S., Saeidi, S., Concepcion, P., et al., 2021. Oxidative dehydrogenation of ethane: catalytic and mechanistic aspects and future trends. Chem. Soc. Rev. 50, 4564–4605. https://doi.org/10.1039/d0cs01518k.

Numan, M., Kim, T., Jo, C., et al., 2020. Ethane dehydrogenation with CO_2 as a soft oxidant over a Cr-TUD-1 catalyst. J. CO_2 Util. 39, 101184. https://doi.org/10.1016/j.jcou.2020.101184.

Numan, M., Eom, E., Li, A., et al., 2021. Oxidative dehydrogenation of ethane with CO_2 as a soft oxidant over a PtCe bimetallic catalyst. ACS Catal. 11, 9221–9232. https://doi.org/10.1021/acscatal.1c01156.

Park, J.L., Canizales, K.A., Argyle, M.D., et al., 2020. The effects of doping alumina with silica in alumina-supported NiO catalysts for oxidative dehydrogenation of ethane. Microporous Mesoporous Mater. 293, 109799. https://doi.org/10.1016/j.micromeso.2019.109799.

Qiu, B., Zhang, Y., Liu, Y., et al., 2021. The state of Pt active phase and its surrounding environment during dehydrogenation of ethane to ethylene. Appl. Surf. Sci. 554, 149611. https://doi.org/10.1016/j.apsusc.2021.149611.

Rahmani, F., Haghighi, M., Mohammadkhani, B., 2017. Enhanced dispersion of Cr nanoparticles over nanostructured ZrO_2-doped ZSM-5 used in CO_2-oxydehydrogenation of ethane. Microporous Mesoporous Mater. 242, 34–49. https://doi.org/10.1016/j.micromeso.2017.01.012.

Shishido, T., Shimamura, K., Teramura, K., et al., 2012. Role of CO_2 in dehydrogenation of propane over Cr-based catalysts. Catal. Today 185, 151–156. https://doi.org/10.1016/j.cattod.2011.10.028.

Tedeeva, M.A., Kustov, A.L., Pribytkov, P.V., et al., 2022. Dehydrogenation of propane in the presence of CO_2 on GaO_x/SiO_2 catalyst: influence of the texture characteristics of the support. Fuel 313, 122698. https://doi.org/10.1016/j.fuel.2021.122698.

Tian, X., Zheng, C., Zhao, H., 2022. Ce-modified $SrFeO_3$- for ethane oxidative dehydrogenation coupled with CO_2 splitting via a chemical looping scheme. Appl. Catal. B Environ. 303, 120894. https://doi.org/10.1016/j.apcatb.2021.120894.

Tian, J., Kong, R., Deng, B., et al., 2024. Non-classical deactivation mechanism in a supported intermetallic catalyst for propane dehydrogenation. Angew. Chem., Int. Ed. Engl. 63, e202409556. https://doi.org/10.1002/anie.202409556.

Wan, T., Jin, F., Cheng, X., et al., 2022. Influence of hydrophilicity and titanium species on activity and stability of Cr/MWW zeolite catalysts for dehydrogenation of ethane with CO_2. Appl. Catal. A: Gen. 637, 118542. https://doi.org/10.1016/j.apcata.2022.118542.

Wang, Y., Ohishi, Y., Shishido, T., et al., 2003. Characterizations and catalytic properties of Cr-MCM-41 prepared by direct hydrothermal synthesis and template-ion exchange. J. Catal. 220, 347–357. https://doi.org/10.1016/s0021-9517(03)00278-1.

Wang, J., Zhu, M.L., Song, Y.H., et al., 2022a. Molecular-level investigation on supported CrO_x catalyst for oxidative dehydrogenation of propane with carbon dioxide. J. Catal. 409, 87–97. https://doi.org/10.1016/j.jcat.2022.03.027.

Wang, J., Song, Y.H., Yuan, E.H., et al., 2022b. Elucidating the support-size effect on the catalytic stability of CrO_x/silicalite-1 for oxidative dehydrogenation of propane with CO_2. Catal. Lett. 153, 790–804. https://doi.org/10.1007/s10562-022-04012-4.

Wang, G., Zhu, C., Zhang, S., et al., 2023. Deactivation origins and stability-enhancing strategies of Sn/SiO_2 catalysts for ethane dehydrogenation. Mol. Catal. 535, 112826. https://doi.org/10.1016/j.mcat.2022.112826.

Wang, Z., Jia, X., Yan, Z., et al., 2024. CrO_x modified particles size and electronic density of Ni catalyst on ZSM-23 for enhanced hydroisomerization performance of long-chain n-alkanes. Fuel 367, 131476. https://doi.org/10.1016/j.fuel.2024.131476.

Yadav, V., Rosenberger, J.M., Bolton, B.K., et al., 2024. Calcium additives enhance coke migration and catalyst stability for Pt-based catalysts in ethane dehydrogenation. J. Catal. 432, 115446. https://doi.org/10.1016/j.jcat.2024.115446.

Yang, G., Yan, X., Chen, Y., et al., 2022. Improved propylene selectivity and superior catalytic performance of Ga-xMg/ZSM-5 catalysts for propane dehydrogenation (PDH) reaction. Appl. Catal. A: Gen. 643, 118778. https://doi.org/10.1016/j.apcata.2022.118778.

Zhang, Y., Chen, M., Wang, W., et al., 2024. A stable Pt modified cobalt tungstate catalyst for CO_2-assisted oxidative dehydrogenation of ethane. Catal. Sci. Technol. 14, 3924–3935. https://doi.org/10.1039/d4cy00399c.

Zheng, Y., Li, J., Zhang, X., et al., 2023a. Effect of CO_2 Co-feeding on the stabilization of atomically dispersed iron species over $MgAl_2O_4$ during ethane dehydrogenation reactions. ACS Catal. 13, 11153–11163. https://doi.org/10.1021/acscatal.3c02029.

Zheng, Y., Zhang, X., Li, J., et al., 2023b. Role of active oxygen species in Fe-doped ZrO_2 catalyst during CO_2 assisted ethane dehydrogenation reaction. J. Catal. 428, 115130. https://doi.org/10.1016/j.jcat.2023.115130.

Zheng, Y., Li, J., Zhang, X., et al., 2024. Evolution of Co species in CO_2-assisted ethane dehydrogenation: competing cleavage of C-H and C-C bonds. ACS Catal. 14, 4749–4759. https://doi.org/10.1021/acscatal.4c00324.

Zhou, W., Felvey, N., Guo, J., et al., 2024. Reduction of cofed carbon dioxide modifies the local coordination environment of zeolite-supported, atomically dispersed chromium to promote ethane dehydrogenation. J. Am. Chem. Soc. 146, 10060–10072. https://doi.org/10.1021/jacs.4c00995.